

# Dynamic phosphoregulation of the cortical actin cytoskeleton and endocytic machinery revealed by real-time chemical genetic analysis

Mariko Sekiya-Kawasaki,<sup>1</sup> Aaron Chris Groen,<sup>1</sup> M. Jamie T.V. Cope,<sup>1</sup> Marko Kaksonen,<sup>1</sup> Hadiya A. Watson,<sup>4</sup> Chao Zhang,<sup>3</sup> Kevan M. Shokat,<sup>3</sup> Beverly Wendland,<sup>4</sup> Kent L. McDonald,<sup>2</sup> J. Michael McCaffery,<sup>5</sup> and David G. Drubin<sup>1</sup>

<sup>1</sup>Department of Molecular and Cell Biology and <sup>2</sup>Electron Microscope Laboratory, University of California, Berkeley, Berkeley, CA 94720

<sup>3</sup>Department of Cellular and Molecular Pharmacology, University of California, San Francisco, San Francisco, CA 94143

<sup>4</sup>Department of Biology and <sup>5</sup>Integrated Imaging Center, The Johns Hopkins University, Baltimore, MD 21218

We used chemical genetics to control the activity of budding yeast Prk1p, which is a protein kinase that is related to mammalian GAK and AAK1, and which targets several actin regulatory proteins implicated in endocytosis. In vivo Prk1p inhibition blocked pheromone receptor endocytosis, and caused cortical actin patches to rapidly aggregate into large clumps that contained Abp1p, Sla2p, Pan1p, Sla1p, and Ent1p. Clump formation depended on Arp2p, suggesting that this phenotype might result from unregulated Arp2/3-stimulated actin assembly. Electron microscopy/immunoelectron microscopy analysis

and tracking of the endocytic membrane marker FM4-64 revealed vesicles of likely endocytic origin within the actin clumps. Upon inhibitor washout, the actin clumps rapidly disassembled, and properly polarized actin patches reappeared. Our results suggest that actin clumps result from blockage at a normally transient step during which actin assembly is stimulated by endocytic proteins. Thus, we revealed tight phosphoregulation of an intrinsically dynamic, actin patch-related process, and propose that Prk1p negatively regulates the actin assembly-stimulating activity of endocytic proteins.

## Introduction

Control of actin dynamics by associated proteins plays a crucial role in many biological processes including endocytosis, exocytosis, organelle inheritance, cell motility, and cell morphogenesis. F-actin in *Saccharomyces cerevisiae* is mainly found in three distinct structures: cables, the contractile ring, and cortical patches (Pruyne and Bretscher, 2000). Actin patches can be highly motile (0.06–1 μm/s) and undergo active turnover (for review see Engqvist-Goldstein and Drubin, 2003). They are also functionally linked to endocytosis, as many actin patch components are essential for this process, and drugs that perturb actin turnover inhibit endocytosis (for review see Engqvist-Goldstein and Drubin, 2003). Consistent with these observations, transient association

between the actin cytoskeleton and endocytic sites has recently been shown to be a characteristic of caveolae- and clathrin-mediated endocytosis in mammalian cells (for review see Engqvist-Goldstein and Drubin, 2003). However, the molecular mechanisms underlying actin's involvement in endocytosis remain poorly understood.

Yeast actin-regulating kinase (Ark) 1p and Prk1p, a redundant pair of Ark family kinases, are strong candidates to directly couple the dynamic processes of actin cytoskeleton assembly and endocytosis (for review see Smythe and Ayscough, 2003). The three known in vivo targets of Prk1p, Pan1p (Eps15-related Arp2/3 activator; Zeng and Cai, 1999; Duncan et al., 2001), Ent1p (epsin-related protein; Watson et al., 2001), and Sla1p (an adaptor for Ste2p receptor endocytosis; Zeng and Cai, 1999; Howard et al., 2002), are actin patch proteins. Each of these Prk1p targets plays an important role in both endocytosis and in actin cytoskeleton regulation

The online version of this article includes supplemental material.

Address correspondence to D.G. Drubin, Dept. of Molecular and Cell Biology, 16 Barker Hall, University of California, Berkeley, Berkeley, CA 94720-3202. Tel.: (510) 642-3692. Fax: (510) 643-0062. email: drubin@uclink4.berkeley.edu

Key words: protein kinases; Eps15; Arp2/3; endocytosis; *Saccharomyces cerevisiae*

Abbreviations used in this paper: 1NA-PP1, 4-amino-1-*tert*-butyl-3-(1'-naphthyl)pyrazolo[3,4-*d*]pyrimidine; Ark, actin-regulating kinase.

(for review see Engqvist-Goldstein and Drubin, 2003). Both elevation and loss of Ark kinase activity lead to defective actin cytoskeleton organization and endocytosis (Cope et al., 1999; Zeng and Cai, 1999; Watson et al., 2001; Zeng et al., 2001), suggesting that the regulation by protein phosphorylation is crucial for both systems. A mammalian Ark family kinase, AAK1, localizes to sites of clathrin-mediated endocytosis, and phosphorylation by AAK1 negatively regulates endocytosis (Conner and Schmid, 2002).

To gain insights into the regulatory mechanisms of actin cytoskeleton assembly and endocytosis by Prk1p, we used a chemical genetics approach (Bishop et al., 2001) that enabled us to rapidly modulate Prk1p activity *in vivo*. In comparison to the conventional approach using kinase-dead mutants, this approach enabled us to investigate the direct and immediate consequence of Prk1p inactivation for the regulation of actin assembly and endocytosis.

## Results and discussion

### Construction of *prk1*-analogue-sensitive (*prk1-as*) mutants that rapidly respond to 1NA-PP1

To determine how Prk1p functions in actin organization and endocytosis in living cells, we created analogue-sensitive mutants (Bishop et al., 2001) of Prk1p in cells that lack Ark1p. Inactivation of both kinases was necessary because either one alone is sufficient to carry out the functions related to actin organization (Cope et al., 1999) and endocytosis (unpublished data). We constructed *ark1Δ prk1-as1* (with a M108G mutation) and *ark1Δ prk1-as3* (with M108G and C175A mutations) strains, in which substitutions of bulky amino acids in the ATP-binding pocket of Prk1p were made to render the kinase sensitive to a PP1 analogue, 4-amino-1-*tert*-butyl-3-(1'-naphthyl)pyrazolo[3,4-*d*]pyrimidine (1NA-PP1; Bishop et al., 1998). In the absence of 1NA-PP1, both *ark1Δ prk1-as1* and *ark1Δ prk1-as3* mutants had growth rates and actin morphologies indistinguishable from the wild-type parent strain, and showed normal growth at 37°C.

*ark1Δ prk1-as1* and *ark1Δ prk1-as3* cells showed specific sensitivity to 1NA-PP1. Upon treatment of these mutants with 1NA-PP1, unpolarized actin and actin clumps were observed in a dose-dependent manner (Fig. 1, A and B), indicating that inhibitor treatment mimics the phenotype seen upon loss of Ark1p and Prk1p (Cope et al., 1999). Actin cables appeared to be unaffected by inhibitor addition (Fig. 1 A; +1NA-PP1). As assessed by quantifying the percentage of cells forming actin clumps, the effect of 1NA-PP1 was saturated at 80 μM for *ark1Δ prk1-as1*, and at 40 μM for *ark1Δ prk1-as3* (Fig. 1 B). As a further indication that *ark1Δ prk1-as3* cells are more sensitive to the inhibitor, at optimal inhibitor doses, 40 μM for *ark1Δ prk1-as3* and 80 μM for *ark1Δ prk1-as1*, ~95% of *ark1Δ prk1-as3* cells formed actin clumps, whereas ~80% of *ark1Δ prk1-as1* cells formed clumps (Fig. 1 B). The actin cytoskeleton of *ark1Δ PRK1* cells was not affected by 40–120 μM 1NA-PP1 (unpublished data).

Next, we analyzed the *in vivo* phosphorylation of Ent1p, a target of Prk1p that shows a Prk1p-dependent mobility shift (Watson et al., 2001). Both *ark1Δ prk1-as1* and *ark1Δ prk1-*

*as3* cells display wild-type Ent1p phosphorylation levels in the absence of 1NA-PP1 (Fig. 1 C). Addition of inhibitor for 30 min resulted in a dose-dependent inhibition of Ent1p phosphorylation in *ark1Δ prk1-as1* cells (Fig. 1 D, bottom). With 80 μM inhibitor, Ent1p phosphorylation was severely inhibited by 5 min, and appeared completely inhibited by 15 min (Fig. 1 E). Ent1p phosphorylation in *ark1Δ PRK1* cells was not affected by 40–120 μM 1NA-PP1 (Fig. 1 D, top). Thus, 1NA-PP1 specifically and rapidly inhibits Prk1p-as kinase activity. Next, we evaluated actin organization as a function of time after Prk1p inhibition (Fig. 1 F). By 2 min, ~60% of the *ark1Δ prk1-as3* cells had lost actin patch polarization and/or had actin clumps. By 20 min, the percentage of the cells with actin clumps reached saturation (~80% for *ark1Δ prk1-as1*, unpublished data; ~95% for *ark1Δ prk1-as3*, Fig. 1 F). Interestingly, at 2 min, the majority of the actin clumps in *ark1Δ prk1-as1* and *ark1Δ prk1-as3* cells were found in the daughter cell. At 5 min, actin clumps were mainly seen in the mother cell.

The Prk1p target Pan1p is an activator of the Arp2/3 complex. By introducing the temperature-sensitive *arp2-1* mutant of an Arp2/3 complex subunit into the *ark1Δ prk1-as3* background, we tested whether Arp2/3-mediated actin assembly is required for clump formation. The *arp2-1* mutant shows significant endocytic defects at the permissive temperature, although it displays normal actin organization (Moreau et al., 1997). The *ark1Δ prk1-as3 arp2-1* cells formed actin clumps much less efficiently (~5%, *n* = 100) than *ark1Δ prk1-as3* cells (~95–100%, *n* = 100) at 25°C (Fig. 1 G). The actin clumps disappeared rapidly in response to the actin monomer sequestering drug latrunculin-A (Ayscough et al., 1997; unpublished data), suggesting that actin turnover is not severely affected by Prk1p inhibition. In total, these data support the possibility that actin clumps are the result of unregulated Arp2/3-stimulated actin assembly.

### Real-time analysis of actin patch dynamics upon Prk1p inhibition

To investigate actin patch dynamics as a function of Prk1p inhibition, we performed real-time analyses of *ark1Δ prk1-as1* cells expressing Abp1-GFP (Fig. 2). Similar results were obtained with *ark1Δ prk1-as3* cells (unpublished data). Abp1p is a component of cortical actin patches (Drubin et al., 1988). Within 1 to 2 min of 1NA-PP1 addition to *ark1Δ prk1-as1* cells, Abp1-GFP patches aggregated into clumps (Fig. 2 A and Video 1, available at <http://www.jcb.org/cgi/content/full/jcb.200305077/DC1>). Once formed in the daughter cell, the actin clumps invariably moved toward the bud neck, and then into the mother cell (Fig. 2 B), consistent with the observation for fixed cells (Fig. 1 F), which exhibited an increase of mother clumps and a decrease of daughter clumps during the time course. The mechanistic basis for this movement is unknown, but does not seem to involve microtubules because the process was not sensitive to the microtubule-depolymerizing drug nocodazole (unpublished data). Within 1 min of Prk1p reactivation by inhibitor washout, the clumps disassembled, and the normal polarized distribution of Abp1 patches was

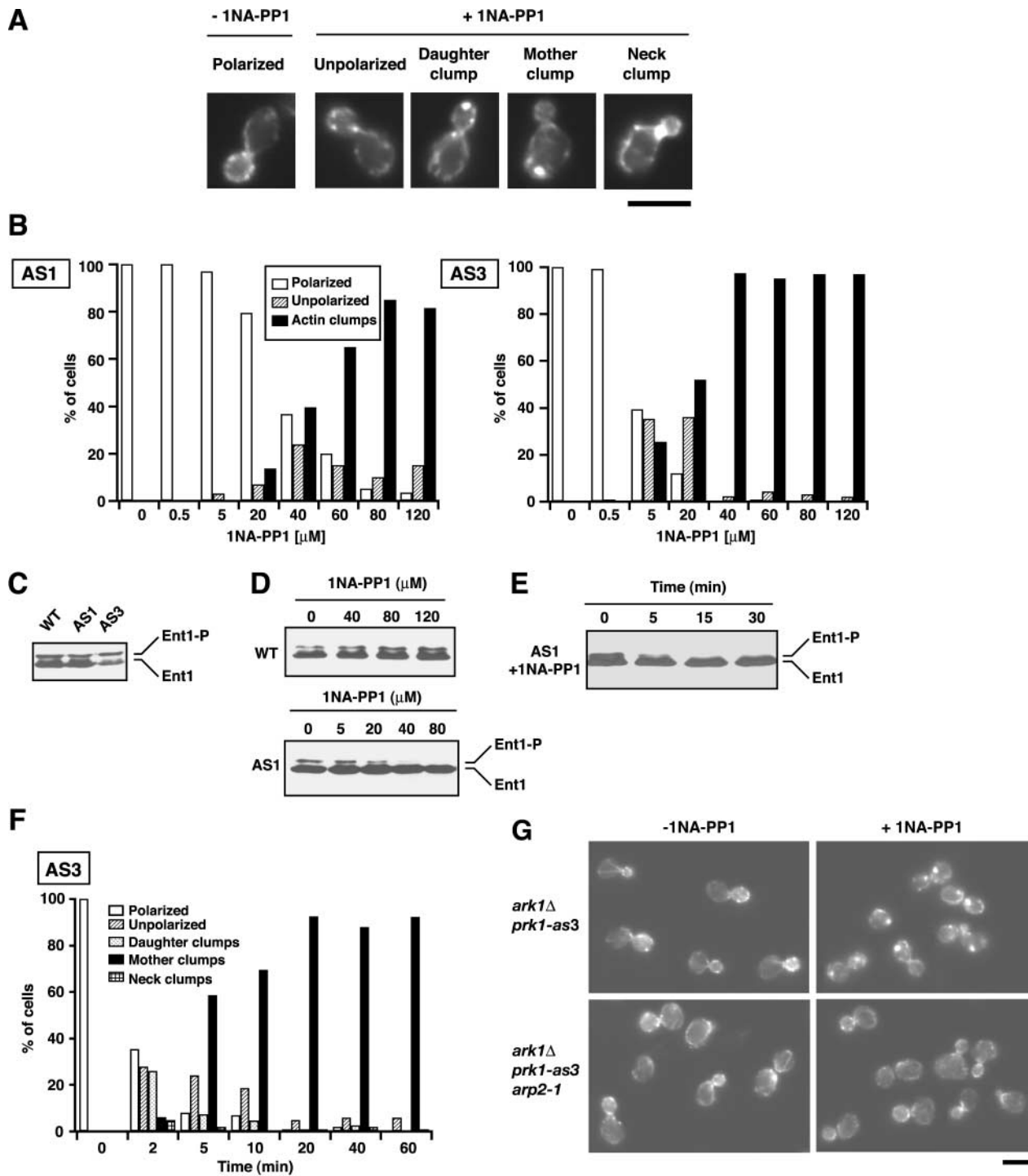
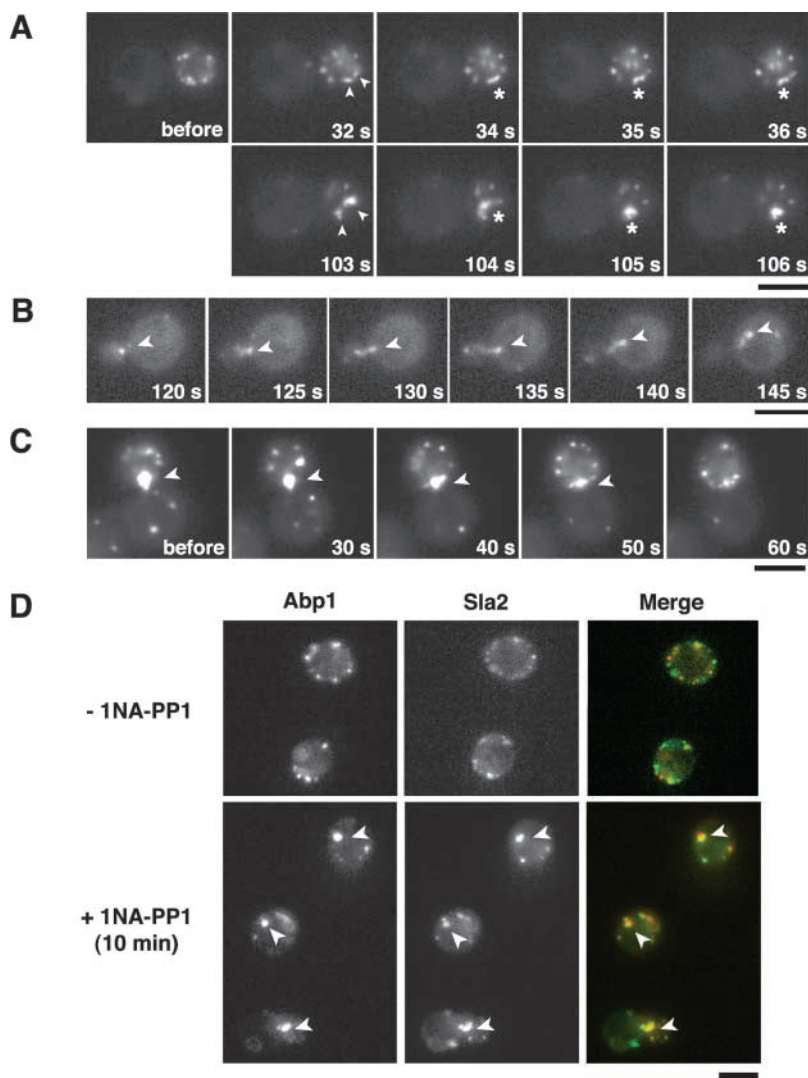


Figure 1. **Initial characterization of *ark1Δ prk1-as* mutants.** (A) To observe the actin morphology, cells were stained with rhodamine-phalloidin. The range of actin morphologies of *ark1Δ prk1-as3* cells treated with 1NA-PP1 for 2 min is shown. A mock-treated cell is also shown. (B) Actin morphology of small-budded *ark1Δ prk1-as1* (AS1) and *ark1Δ prk1-as3* (AS3) cells was scored as a function of 1NA-PP1 concentration in a blind study ( $n \geq 200$  for each sample). The cells were treated with the inhibitor for 1 h before fixation. (C and D) *ark1Δ PRK1* (WT), *ark1Δ prk1-as1*, and *ark1Δ prk1-as3* cells were cultured without 1NA-PP1 (C), or with the indicated concentration of 1NA-PP1 for 30 min (D), and then processed for anti-Ent1p Western blotting. (E) Ent1 phosphorylation as a function of time in *ark1Δ prk1-as1* cells treated with 80  $\mu$ M 1NA-PP1. (C–E) Phosphorylated (Ent1-P) and unphosphorylated (Ent1) forms of Ent1p are indicated. (F) Actin morphology of small-budded *ark1Δ prk1-as3* cells in the presence of 40  $\mu$ M 1NA-PP1 at indicated time points ( $n \geq 100$ ). (G) Actin morphology of *ark1Δ prk1-as3* and *ark1Δ prk1-as3 arp2-1*. The cells were mock treated or treated with 1NA-PP1 at 25°C for 15 min before fixation. Strains: *ark1Δ PRK1*, DDY2547; *ark1Δ prk1-as1*, DDY2595; *ark1Δ prk1-as3*, DDY2597; *ark1Δ prk1-as3 arp2-1*, DDY2610. Bars, 5  $\mu$ m.



**Figure 2. Reversible actin clump formation from cortical actin patches upon inhibition of Prk1p activity.** A and C are the selected frames from Video 1 and Video 2, respectively. (A–C) *ark1Δ prk1-as1* cells expressing Abp1-GFP were imaged. (A and B) Cells before or after treatment with 1NA-PP1 for the indicated times. (A) The two Abp1 patches (top, arrowheads) or already formed clumps (bottom, arrowheads) fuse to become one entity (asterisks) upon addition of 1NA-PP1. (B) An Abp1 clump (arrowhead) moves from the daughter to the mother cell. (C) Cells were pretreated with 1NA-PP1 for 30 min, followed by washout of the inhibitor. An Abp1 clump at the neck (arrowhead) disappears during the time course. (D) *ark1Δ prk1-as1* cells expressing Abp1-CFP (red) and Sla2-YFP (green) were imaged after a 10-min treatment with 1NA-PP1. Mock-treated cells are also shown. The actin clumps are marked with arrowheads. Exposure times for each panel: 1 s for A and C, 66 ms for B, and 300–700 ms for D. Strains: *ark1Δ prk1-as1 ABP1-GFP*, DDY2600 (A and C) and DDY2601 (B); *ark1Δ prk1-as1 ABP1-CFP SLA2-YFP*, DDY2603 (D). Bars, 5  $\mu$ m.

restored (Fig. 2 C and Video 2). Rhodamine-phalloidin staining of fixed *ark1Δ prk1-as1* cells confirmed that F-actin undergoes reversible aggregation upon 1NA-PP1 addition (unpublished data).

The endocytic proteins Sla2p, Pan1p, Sla1p, and Ent1p, which localize at actin patches in wild-type cells, were previously shown to be present in the large actin clumps in *ark1Δ prk1Δ* cells (Cope et al., 1999; Watson et al., 2001; Warren et al., 2002). We found that all of these proteins are also present in the inhibitor-induced clumps (Fig. 2 D for Sla2p; unpublished data for Pan1p, Sla1p, and Ent1p). The rapid and reversible actin clump formation described in Figs. 1 and 2 revealed that the wild-type actin patches are under tight regulation by protein phosphorylation. Several lines of evidence support the conclusion that actin clump formation is a direct consequence of inhibiting phosphorylation of actin patch components. First, all known *in vivo* targets (Pan1p, Sla1p, and Ent1p) of Prk1p are actin patch proteins. Second, Prk1p kinase is exclusively localized in cortical actin patches (Cope et al., 1999; Zeng and Cai, 1999). Third, actin clumps form rapidly upon addition of 1NA-PP1, and disappear rapidly when it is removed.

### Receptor-mediated endocytic internalization is blocked upon Prk1p inhibition

Further, we tested whether Prk1p kinase activity is required for  $\alpha$ -factor internalization by its receptor, Ste2p. Because of its high sensitivity to 1NA-PP1, all subsequent analyses used the *prk1-as3* allele. Without inhibitor, *ark1Δ prk1-as3* cells show internalization kinetics indistinguishable from *ark1Δ PRK1* (Fig. 3 A). Treatment of *ark1Δ prk1-as3* cells with 1NA-PP1 for 30 min specifically inhibited receptor internalization (Fig. 3 B). Even 120  $\mu$ M inhibitor did not affect  $\alpha$ -factor internalization by *ark1Δ PRK1* cells (Fig. 3 B). Additionally, a kinase-dead mutant (*ark1Δ prk1<sup>D159A</sup>*) also showed a severe block of receptor internalization (Fig. 3 C). Thus, the inhibition of Prk1p kinase activity profoundly blocks the internalization step of receptor-mediated endocytosis.

### Association of endocytic membranes with actin upon Prk1p inhibition

Next, we investigated the fate of the endocytic membrane marker FM4-64 (Vida and Emr, 1995) in inhibitor-treated *ark1Δ prk1-as3* cells (Fig. 4). FM4-64 was first incorporated

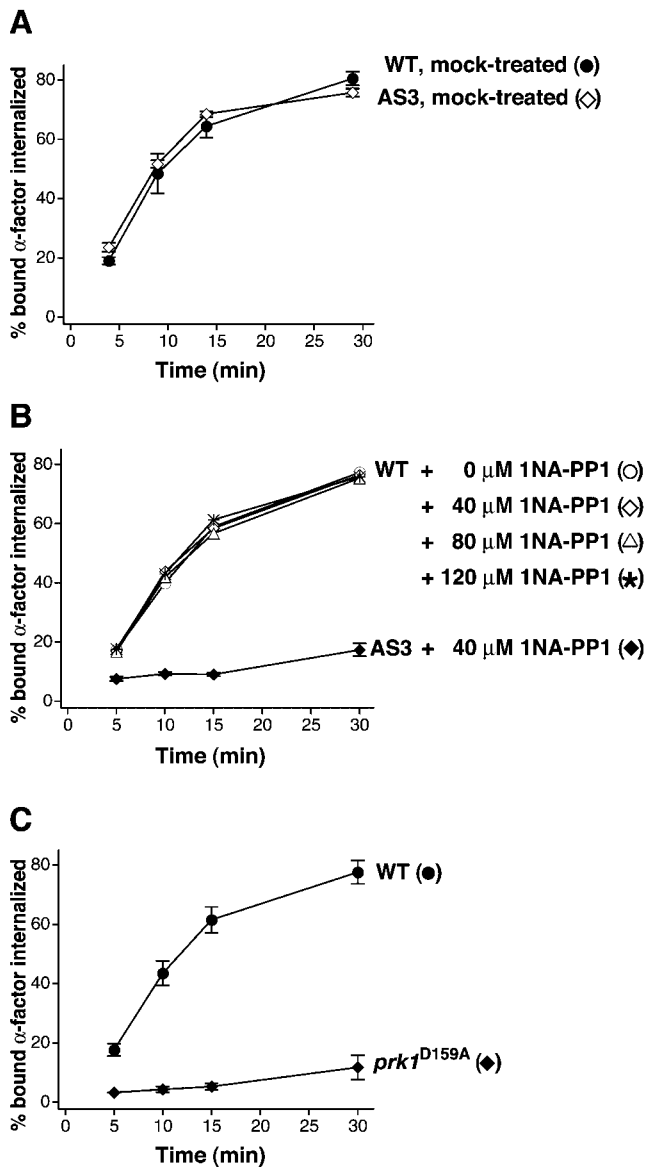


**Figure 3. Defective receptor-mediated endocytosis upon inhibition of Prk1p activity.** Internalization of  $^{35}\text{S}$ -labeled  $\alpha$ -factor was measured. In A and B, the time course of internalization was started after 30 min incubation with 1NA-PP1 or mock treatment. (A) *ark1 $\Delta$  PRK1* (WT) and *ark1 $\Delta$  prk1-as3* (AS3) cells without 1NA-PP1. (B) *ark1 $\Delta$  PRK1* (WT) and *ark1 $\Delta$  prk1-as3* (AS3) cells treated with 1NA-PP1. (C) *ark1 $\Delta$  PRK1* (WT) and *ark1 $\Delta$  prk1<sup>D159A</sup>* (*prk1<sup>D159A</sup>*) cells. Error bars represent the SD from at least three experiments. The experiment with *ark1 $\Delta$  PRK1* in B was performed twice. Strains: *ark1 $\Delta$  PRK1*, DDY2607; *ark1 $\Delta$  prk1-as3*, DDY2608; *ark1 $\Delta$  prk1<sup>D159A</sup>*, DDY2609.

into the plasma membrane (Fig. 4 A, 0 min). In mock-treated *ark1 $\Delta$  prk1-as3* or wild-type cells, this dye is later found in endosomes (Fig. 4 A, top, 5 min) and finally accumulates in vacuoles (Vida and Emr, 1995; unpublished data). In mock-treated cells, the endosomes seen at 5 min do not show significant colocalization with Abp1p (Fig. 4 A, top). Next, we treated *ark1 $\Delta$  prk1-as3* cells simultaneously with FM4-64 and 1NA-PP1. At 5 min, we found that FM4-64 staining colocalized with actin clumps (Fig. 4 A, bottom). The FM4-64 dye in actin clumps was later transported to vacuoles (after 15–20 min), although the kinetics

were delayed compared with the wild type (10 min; unpublished data). These observations suggest that the block of Prk1p activity leads to accumulation of an endocytic compartment that associates with actin.

Next, we examined *ark1 $\Delta$  prk1 $\Delta$*  (Fig. 4, C–H and K–N) and inhibitor-treated *ark1 $\Delta$  prk1-as3* cells (Fig. 4, I and J for cells treated for 10 min; also see Fig. S1) by conventional EM. To better visualize actin filaments, we first observed cells post-treated with tannic acid (Fig. 4, B–J). Compared with wild-type cells that showed no remarkable morphology (Fig. 4 B), both *ark1 $\Delta$  prk1 $\Delta$*  and inhibitor-treated *ark1 $\Delta$  prk1-as3* cells showed clustered vesicles of  $\sim 100$  nm (arrows) in the area where microfilaments (arrowheads) are observed (Fig. 4, C–J, dashed area; also see Fig. S1). Next, we observed *ark1 $\Delta$  prk1 $\Delta$*  cells processed by high pressure freezing followed by freeze substitution, and also detected accumulation of  $\sim 100$ -nm vesicles (Fig. 4, K–N, arrows). With this procedure, the vesicles are seen within areas that exclude ribosomes (Fig. 4 K, dashed area), and they sometimes appear to have electron-dense coats (Fig. 4 M, left arrow; Fig. 4 N, arrow). The colocalization of vesicles with microfilaments and ribosome exclusion areas suggested that the vesicles might reside within actin clumps. Therefore, we used immuno-EM to determine if this was indeed the case (Fig. 4, O–R). In indirect immunolabeling for actin on ultrathin cryosections of fixed *ark1 $\Delta$  prk1 $\Delta$*  cells, 10-nm gold particles were seen to localize to slightly electron-dense areas (Fig. 4 O, dashed area). These immunogold-labeled actin clumps were seen to contain  $\sim 100$ -nm vesicles similar to those seen using conventional EM (Fig. 4, O–Q, dashed boxes). Thus, we conclude that the block of the Ark kinases leads to the accumulation of actin and actin-associated vesicles. Additionally, in double-immunogold labeling for Sla1-GFP (5-nm gold) and actin (10-nm gold), Sla1-containing vesicles were occasionally detected within the actin clumps (Fig. 4 R).

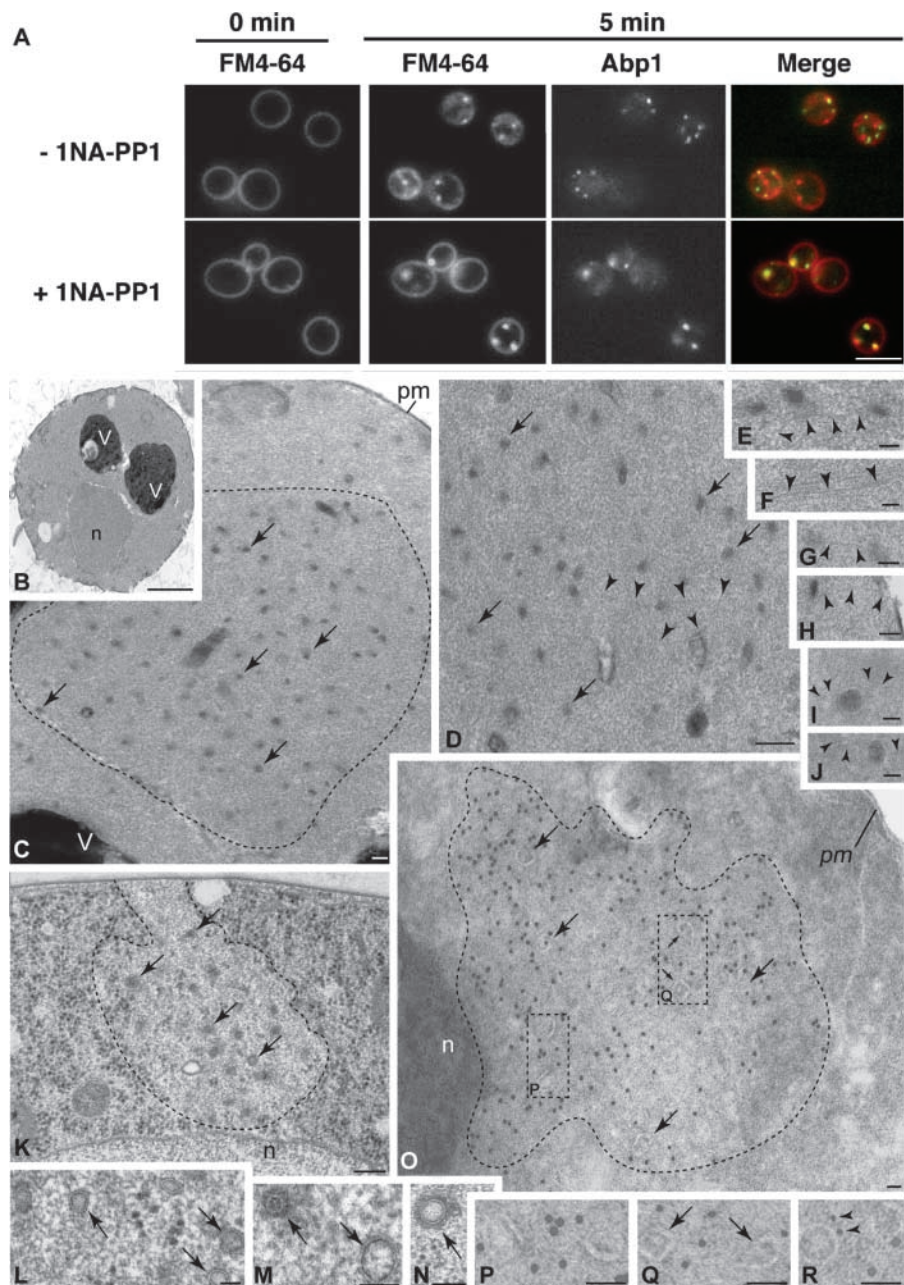
In this work, we examined the rapid and acute effects of Prk1p kinase inhibition and reactivation by applying a chemical genetics approach. We showed that abnormal actin clumps formed and disappeared within 1 to 2 min of Prk1p inhibition and reactivation, respectively. Further, we showed that the actin clumps contain endocytic proteins and  $\sim 100$ -nm vesicles. We propose that Prk1p directly regulates the coupling between actin assembly and endocytosis by promoting disassembly and/or inactivation of an early endocytic complex that stimulates actin assembly (Fig. 5 A). When Prk1p is inhibited, this complex is stabilized, and actin assembly continues to be stimulated by endocytic proteins such as the Prk1p target Pan1p and the associated Arp2/3 complex (Zeng and Cai, 1999; Duncan et al., 2001), and/or other targets including Sla1p and Ent1p (Watson et al., 2001; Zeng et al., 2001; Fig. 5 B). In mammalian cells, the  $\mu 2$  subunit of AP2 is phosphorylated by AAK1 at Thr-156 (ITSQVT<sup>156</sup>G) (Ricotta et al., 2002). However, the budding yeast AP2 homologue, Apm4p (Huang et al., 1999), is not important for receptor internalization and does not contain potential Prk1p-phosphorylation motifs similar to (L/IxxQxTG). Rather, our genetic experiment showing that Arp2p is required for clump formation supports the idea that Arp2/3-mediated actin assembly is negatively regulated by Prk1p, potentially via phosphorylation of the Arp2/3 ac-

### Figure 4. Actin-associated membrane accumulation upon inhibition of Prk1p activity.

(A) FM4-64 labeling of *ark1Δ prk1-as3* cells expressing Abp1-GFP. Cells were treated with media containing FM4-64 and 1NA-PP1 in a flow chamber. FM4-64 (red) and Abp1-GFP (green) were visualized at 0 and 5 min. Mock-treated cells are also shown. (B–J) Conventional EM of cells post-treated with 1% tannic acid. (B) A wild-type cell shows normal, unremarkable morphology. (C–H) *ark1Δ prk1Δ* cells reveal electron-dense areas (encircled by dashed line in C) containing a heterogeneous population of ~100-nm vesicles (shown at higher magnification in D and indicated by arrows in C and D), as well as numerous microfilament profiles (marked by arrowheads in D–H). (I and J) *ark1Δ prk1-as3* cells treated with 1NA-PP1 for 10 min also reveal ~100-nm vesicles and microfilament profiles (marked by arrowheads).

For more examples, also see Fig. S1. (K–N) EM of cells fixed by high pressure freezing and freeze substitution. *ark1Δ prk1Δ* cells reveal ribosome exclusion areas (encircled by dashed line in K) containing ~100-nm vesicles (some of which are indicated by arrows in K–N). Ribosomes appear as small, uniform, electron-dense spots distributed throughout most of the cytoplasm. (O–Q) Indirect immunogold labeling of ultrathin cryosections of *ark1Δ prk1Δ* cells demonstrates the localization of actin within a slightly electron-dense/vesicle-enriched region (encircled by dashed line in O). In many instances, vesicles/membranous elements are detected within actin-labeled region (arrows in O and Q; boxed areas P and Q).

(R) Double-indirect immunogold labeling with *ark1Δ prk1Δ SLA1-GFP* cells reveals occasional Sla1p-containing vesicles (5-nm gold, arrowheads) amid a clustered/electron-dense actin region (10-nm gold). Strains: *ark1Δ prk1-as3 ABP1-GFP*, DDY2606 (A); Wild-type, DDY904 (B); *ark1Δ prk1Δ*, DDY2541 (C–H and O–Q) and DDY1564 (K–N); *ark1Δ prk1-as3*, DDY2597 (I and J); *ark1Δ prk1Δ SLA1-GFP*, DDY2611 (R). *n*, nucleus; *V*, vacuole; *pm*, plasma membrane. Bars: (A) 5 μm; (B) 1 μm; (C) 0.2 μm; (D) 0.5 μm; (E–J) 0.1 μm; (K) 0.5 μm; (L–R) 0.1 μm.



tivator, Pan1p. Our data also support the proposal that actin participates directly in yeast endocytosis.

## Materials and methods

### Media, growth conditions, and materials

Yeast strains were grown in standard rich media (YPD) or synthetic media (SD) supplemented with the appropriate amino acids. 1NA-PP1 was synthesized and handled as described previously (Bishop et al., 1998). *ark1Δ prk1-as1* cells were treated with 80 μM inhibitor and *ark1Δ prk1-as3* cells with 40 μM inhibitor in SD-based media unless indicated otherwise. All the yeast strains were cultured at 25°C, except for DDY904 and *ark1Δ prk1Δ*, which were cultured at 30°C.

### Strains and plasmids

The yeast strains are listed in Table I. *prk1Δ::PRK1::URA3* and *prk1Δ::prk1::URA3* integration plasmids were created as follows: First, a NotI site

was introduced 249 bp upstream of the *PRK1* ORF. The mutated KpnI/SacI *PRK1* fragment was cloned into pBlueScript<sup>®</sup> II SK, and the *PRK1* fragment was marked with *URA3* at NotI to create a plasmid pDD877. *prk1-as1* (M108G), *prk1-as3* (M108G, C175A), and *prk1<sup>D159A</sup>* mutations were created in pDD877. The *URA3*-marked, *PRK1*-containing fragments were excised from the integration plasmids, and replaced the *prk1Δ::LEU2* locus. These strains were each crossed with an *ark1Δ* strain, and the diploids were sporulated to obtain *ark1Δ prk1* mutants. Analogue-sensitive Prk1 mutant proteins were expressed at normal levels, but Prk1<sup>D159A</sup>p was expressed at only 20–30% of normal levels at 25°C. The gene deletions were created as described previously (Cope et al., 1999). Functional GFP and CFP tags were integrated at the COOH terminus of Abp1p and Sla1p as described previously (Warren et al., 2002). To create Sla2-YFP, five alanines were introduced at the junction between the *SLA2* ORF and YFP using pDH5 (from the Yeast Resource Center, Seattle, WA). The Sla2-YFP strain has growth properties that are indistinguishable from the wild type. pDD890 expresses Abp1-GFP from pRB2139 (Doyle and Botstein, 1996) on pRS317.

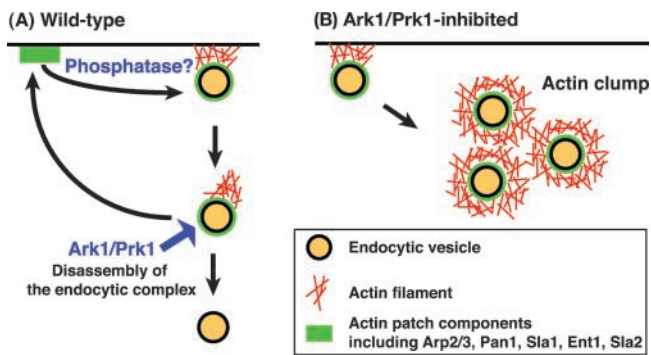


Figure 5. **Model for Ark-kinase function in endocytosis.** (A) In wild-type cells, Prk1p promotes proper disassembly of the actin-associated endocytic complex. Phosphatase(s) might be responsible for reformation and/or activation of the endocytic complex. Ark1p, a closely related homologue of Prk1p, is likely to perform an overlapping function. (B) When Ark1p and Prk1p are inhibited, vesicles associated with actin filaments and endocytic proteins accumulate. See text for further discussion.

### Fluorescent microscopy

F-actin was stained as described previously (Cope et al., 1999). FM4-64 was used at a concentration of 8  $\mu\text{M}$  in SD-based media. For live imaging, cells were attached to 50  $\mu\text{g}/\text{ml}$  concanavalin A-coated long coverslips (24  $\times$  50 mm). A flow chamber was made by mounting a small coverslip (18  $\times$  18 mm) on top of the long coverslip with grease and small pieces of coverslips as spacers. Two sides were left unsealed so that media could be exchanged. Cells were viewed using a microscope (model TE300; Nikon)

equipped with a 100 $\times$  objective, NA 1.4, and a cooled CCD camera (Hamamatsu). Phase-3 software (Phase-3 Imaging Systems) was used for visualization of rhodamine, GFP, and FM4-64. In a CFP-YFP colocalization study, cells were photographed by rapidly alternating excitation/emission filters (JP4 filter sets; Chroma Technology Corp.). Filter wheels (Lambda 10-2; Sutter Instrument Co.) were mounted on the excitation and emission ports of the microscope and were controlled with MetaMorph<sup>®</sup> software (Universal Imaging Corp.).

### Electron microscopy

Morphological observations of cells by conventional EM was performed essentially as described previously (Rieder et al., 1996), except that after fixation with  $\text{Fe}(\text{CN})_2\text{O}_4/\text{thiocarbohydrazide}/\text{Fe}(\text{CN})_2\text{O}_4$  (OTO), the cells were further treated with 1% tannic acid for 30 min. Morphological observations of cells fixed by high pressure freezing and freeze substitution were performed as described in McDonald and Müller-Reichert (2002). Immuno-EM was performed as described previously (Rieder et al., 1996). Primary antibodies used were affinity-purified rabbit anti-actin antibody (a gift from A. Bretscher, Cornell University, Ithaca, NY) and mouse anti-GFP antibody (StressGen Biotechnologies); secondary 5- and 10-nm gold conjugates were obtained from Jackson Immunoresearch Laboratories.

### Protein and immunological techniques

To obtain yeast whole-cell lysates, the cells were lysed with glass beads in ice-cold lysis buffer (50 mM Tris-HCl, pH 7.5, 150 mM NaCl, 1% NP-40, protease inhibitor cocktail, 50 mM NaF, 0.2 mM sodium orthovanadate, 25 mM  $\beta$ -glycerophosphate, 1  $\mu\text{M}$  cyclosporin A, 4 and 0  $\mu\text{M}$  cantharidin). 50  $\mu\text{g}$  of the lysate was loaded per lane. For the time-course experiment, 2-OD cells were harvested and resuspended in 50  $\mu\text{l}$  lysis buffer (50 mM Tris, pH 6.8, 2% SDS, 100 mM DTT, 8% glycerol, 0.02% BPB, protease inhibitor cocktail, 50 mM NaF, 0.2 mM sodium orthovanadate, 25 mM  $\beta$ -glycerophosphate, and 1  $\mu\text{M}$  cyclosporin A). The suspension was boiled for 3 min, and then lysed with glass beads for 2 min, followed by 1 min of boiling. 100  $\mu\text{l}$  of the SDS-PAGE buffer was finally added to the lysate. 10

Table I. Yeast strains

Strain	Genotype	Source
DDY426	<i>MAT<math>\alpha</math>/MAT<math>\alpha</math> his3-<math>\Delta</math>200/his3-<math>\Delta</math>200 leu2-3, 112/leu2-3, 112 ura3-52/ura3-52 ade2-1/ADE2 lys2-801/lys2-801</i>	Drubin lab
DDY904 <sup>b</sup>	<i>MAT<math>\alpha</math> his3-<math>\Delta</math>200 leu2-3, 112 ura3-52 lys2-801</i>	Drubin lab
DDY1102	<i>MAT<math>\alpha</math>/MAT<math>\alpha</math> his3-<math>\Delta</math>200/his3-<math>\Delta</math>200 leu2-3, 112/leu2-3, 112 ura3-52/ura3-52 ade2-1/ADE2 lys2-801/LYS2</i>	Drubin lab
DDY1564 <sup>a</sup>	<i>MAT<math>\alpha</math> his3-<math>\Delta</math>200 leu2-3, 112 ura3-52 lys2-801 ark1<math>\Delta</math>::HIS3 prk1<math>\Delta</math>::LEU2</i>	Drubin lab
DDY2541 <sup>b</sup>	<i>MAT<math>\alpha</math> his3-<math>\Delta</math>200 leu2-3, 112 ura3-52 lys2-801 ark1<math>\Delta</math>::cgHIS3<sup>c</sup> prk1<math>\Delta</math>::cgLEU2<sup>c</sup></i>	This work
DDY2547 <sup>b</sup>	<i>MAT<math>\alpha</math> his3-<math>\Delta</math>200 leu2-3, 112 ura3-52 lys2-801 ark1<math>\Delta</math>::cgHIS3<sup>c</sup> prk1<math>\Delta</math>::PRK1::URA3</i>	This work
DDY2595 <sup>b</sup>	<i>MAT<math>\alpha</math> his3-<math>\Delta</math>200 leu2-3, 112 ura3-52 lys2-801 ark1<math>\Delta</math>::cgHIS3<sup>c</sup> prk1<math>\Delta</math>::prk1-as1::URA3</i>	This work
DDY2597 <sup>b</sup>	<i>MAT<math>\alpha</math> his3-<math>\Delta</math>200 leu2-3, 112 ura3-52 lys2-801 ark1<math>\Delta</math>::cgHIS3<sup>c</sup> prk1<math>\Delta</math>::prk1-as3::URA3</i>	This work
DDY2600 <sup>a</sup>	<i>MAT<math>\alpha</math> his3-<math>\Delta</math>200 ura3-52 leu2-3, 112 lys2-801 ark1<math>\Delta</math>::LEU2 prk1<math>\Delta</math>::prk1-as1::URA3 ABP1-GFP::HIS3</i>	This work
DDY2601 <sup>a</sup>	<i>MAT<math>\alpha</math> his3-<math>\Delta</math>200 ura3-52 leu2-3, 112 lys2-801 ark1<math>\Delta</math>::LEU2 prk1<math>\Delta</math>::prk1-as1::URA3 with pDD890 [CEN, LYS2, ABP1-GFP]</i>	This work
DDY2603 <sup>a</sup>	<i>MAT<math>\alpha</math> his3-<math>\Delta</math>200 ura3-52 leu2-3, 112 lys2-801 ark1<math>\Delta</math>::LEU2 prk1<math>\Delta</math>::prk1-as1::URA3 ABP1-CFP::KanMX6 SLA2-YFP::HIS3</i>	This work
DDY2606 <sup>b</sup>	<i>MAT<math>\alpha</math> his3-<math>\Delta</math>200 ura3-52 leu2-3, 112 lys2-801 ark1<math>\Delta</math>::cgHIS3<sup>c</sup> prk1<math>\Delta</math>::prk1-as3::URA3 ABP1-GFP::HIS3</i>	This work
DDY2607 <sup>a</sup>	<i>MAT<math>\alpha</math> his3-<math>\Delta</math>200 ura3-52 leu2-3, 112 lys2-801 ark1<math>\Delta</math>::HIS3 prk1<math>\Delta</math>::PRK1::URA3 bar1<math>\Delta</math>::cgLEU2<sup>c</sup></i>	This work
DDY2608 <sup>a</sup>	<i>MAT<math>\alpha</math> his3-<math>\Delta</math>200 ura3-52 leu2-3, 112 lys2-801 ark1<math>\Delta</math>::HIS3 prk1<math>\Delta</math>::prk1-as3::URA3 bar1<math>\Delta</math>::cgLEU2<sup>c</sup></i>	This work
DDY2609 <sup>a</sup>	<i>MAT<math>\alpha</math> his3-<math>\Delta</math>200 ura3-52 leu2-3, 112 lys2-801 ark1<math>\Delta</math>::HIS3 prk1<math>\Delta</math>::prk1<sup>D159A</sup>::URA3 bar1<math>\Delta</math>::cgLEU2<sup>c</sup></i>	This work
DDY2610 <sup>b</sup>	<i>MAT<math>\alpha</math> his3-<math>\Delta</math>200 leu2-3, 112 ura3-52 lys2-801 ark1<math>\Delta</math>::cgHIS3<sup>c</sup> prk1<math>\Delta</math>::prk1-as3::URA3 arp2-1::URA3<sup>d</sup></i>	This work
DDY2611 <sup>b</sup>	<i>MAT<math>\alpha</math> his3-<math>\Delta</math>200 leu2-3, 112 ura3-52 lys2-801 ark1<math>\Delta</math>::cgHIS3<sup>c</sup> prk1<math>\Delta</math>::cgLEU2<sup>c</sup> SLA1-GFP::HIS3</i>	This work

<sup>a</sup>Derived from DDY426.

<sup>b</sup>Derived from DDY1102.

<sup>c</sup>cgHIS3 and cgLEU2 indicate *Candida glabrata* HIS3 and LEU2 genes, respectively.

<sup>d</sup>arp2-1 allele (Moreau et al., 1997) was crossed into our strain background.

$\mu$ l of the final supernatant was loaded per lane. Anti-Ent1p antibody (Watson et al., 2001) was used at 1:10,000 dilution for Western blotting.

#### $\alpha$ -factor uptake assay

$^{35}$ S-labeled  $\alpha$ -factor was prepared as described in Howard et al. (2002). The  $\alpha$ -factor uptake assay was performed at 25°C based on a continuous incubation protocol (Dulic et al., 1991) with modifications as follows: cells were grown in SD, harvested by centrifugation, and resuspended in internalization media (SD media with 0.5% casamino acid and 1% BSA). Then the cells were mixed with an equal volume of SD media containing 2 $\times$  concentration of 1NA-PP1. After incubation with 1NA-PP1 for 30 min, 30,000 cpm/100  $\mu$ l  $^{35}$ S-labeled  $\alpha$ -factor was added at time zero. At the indicated time points, aliquots were withdrawn and diluted in ice-cold buffer at pH 6.0 (total  $\alpha$ -factor) or pH 1.1 (internalized  $\alpha$ -factor). The samples were then filtered, and radioactivity was measured in a scintillation counter. The results were expressed as the ratio of pH 1.1 cpm/pH 6.0 cpm for each time point to represent the percentage of internalization.

#### Online supplemental material

Video 1 and Video 2 show *ark1 $\Delta$  prk1-as1* cells expressing Abp1-GFP. The representative frames of the movies are shown in Fig. 2 A and Fig. 2 C. Fig. S1 shows EM of *ark1 $\Delta$  prk1-as3* cells post-treated with tannic acid. Online supplemental material available at <http://www.jcb.org/cgi/content/full/jcb.200305077/DC1>.

We thank James Howard and Gregory Payne for technical assistance and helpful discussion regarding the  $\alpha$ -factor uptake assay; Barbara Winsor (Institut de Biologie Moléculaire et Cellulaire, Strasbourg, France) for providing the *arp2-1* strain and Anthony Bretscher for providing the anti-actin antibody. We also thank the members in Drubin lab for helpful discussions, and Daria Siekhaus and Adam Martin for critical reading of the manuscript.

This work was supported by National Institutes of Health grants to D.G. Drubin (GM42759 and GM50399) and to K.M. Shokat (AI44009); an NIH grant (GM60979) and a Burroughs Wellcome Fund New Investigator Award to B. Wendland; and a National Science Foundation grant (DBI 0099705) to B. Wendland and J.M. McCaffery.

Submitted: 15 May 2003

Accepted: 21 July 2003

## References

- Ayscough, K.R., J. Stryker, N. Pokala, M. Sanders, P. Crews, and D.G. Drubin. 1997. High rates of actin filament turnover in budding yeast and roles for actin in establishment and maintenance of cell polarity revealed using the actin inhibitor latrunculin-A. *J. Cell Biol.* 137:399–416.
- Bishop, A.C., K. Shah, Y. Liu, L. Witucki, C. Kung, and K.M. Shokat. 1998. Design of allele-specific inhibitors to probe protein kinase signaling. *Curr. Biol.* 8:257–266.
- Bishop, A.C., O. Buzko, and K.M. Shokat. 2001. Magic bullets for protein kinases. 2001. *Trends Cell Biol.* 11:167–172.
- Conner, S.D., and S.L. Schmid. 2002. Identification of an adaptor-associated kinase, AAK1, as a regulator of clathrin-mediated endocytosis. *J. Cell Biol.* 156:921–929.
- Cope, M.J., S. Yang, C. Shang, and D.G. Drubin. 1999. Novel protein kinases Ark1p and Prk1p associate with and regulate the cortical actin cytoskeleton in budding yeast. *J. Cell Biol.* 144:1203–1218.
- Doyle, T., and D. Botstein. 1996. Movement of yeast cortical actin cytoskeleton visualized in vivo. *Proc. Natl. Acad. Sci. USA.* 93:3886–3891.
- Drubin, D.G., K.G. Miller, and D. Botstein. 1988. Yeast actin-binding proteins: evidence for a role in morphogenesis. *J. Cell Biol.* 107:2551–2561.
- Dulic, V., M. Egerton, I. Elguindi, S. Raths, B. Singer, and H. Riezman. 1991. Yeast endocytosis assays. *Methods Enzymol.* 194:697–710.
- Duncan, M.C., M.J. Cope, B.L. Goode, B. Wendland, and D.G. Drubin. 2001. Yeast Eps15-like endocytic protein, Pan1p, activates the Arp2/3 complex. *Nat. Cell Biol.* 3:687–690.
- Engqvist-Goldstein, A.E.Y., and D.G. Drubin. 2003. Actin assembly and endocytosis: from yeast to mammals. *Annu. Rev. Cell Dev. Biol.* 19:287–332.
- Howard, J.P., J.L. Hutton, J.M. Olson, and G.S. Payne. 2002. Sla1p serves as the targeting signal recognition factor for NPF<sub>(1,2)</sub>D-mediated endocytosis. *J. Cell Biol.* 157:315–326.
- Huang, K.M., K. D'Hondt, H. Riezman, and S.K. Lemmon. 1999. Clathrin functions in the absence of heterotetrameric adaptors and AP180-related proteins in yeast. *EMBO J.* 18:3897–3908.
- McDonald, K., and T. Müller-Reichert. 2002. Cryomethods for thin section electron microscopy. *Methods Enzymol.* 351:96–123.
- Moreau, V., J.M. Galan, G. Devilliers, R. Haguenaer-Tsapis, and B. Winsor. 1997. The yeast actin-related protein Arp2p is required for the internalization step of endocytosis. *Mol. Biol. Cell.* 8:1361–1375.
- Pruyne, D., and A. Bretscher. 2000. Polarization of cell growth in yeast. II. *J. Cell Sci.* 113:571–585.
- Ricotta, D., S.D. Conner, S.L. Schmid, K. von Figura, and S. Honing. 2002. Phosphorylation of the AP2  $\mu$  subunit by AAK1 mediates high affinity binding to membrane protein sorting signals. *J. Cell Biol.* 156:791–795.
- Rieder, S.E., L.M. Banta, K. Kohrer, J.M. McCaffery, and S.D. Emr. 1996. Multilamellar endosome-like compartment accumulates in the yeast vps28 vacuolar protein sorting mutant. *Mol. Biol. Cell.* 7:985–999.
- Smythe, E., and K.R. Ayscough. 2003. The Ark1/Prk1 family of protein kinases. *EMBO Rep.* 4:246–251.
- Vida, T.A., and S.D. Emr. 1995. A new vital stain for visualizing vacuolar membrane dynamics and endocytosis in yeast. *J. Cell Biol.* 128:779–792.
- Warren, D.T., P.D. Andrews, C.W. Gourlay, and K.R. Ayscough. 2002. Sla1p couples the yeast endocytic machinery to proteins regulating actin dynamics. *J. Cell Sci.* 115:1703–1715.
- Watson, H.A., M.J. Cope, A.C. Groen, D.G. Drubin, and B. Wendland. 2001. In vivo role for actin-regulating kinases in endocytosis and yeast epsin phosphorylation. *Mol. Biol. Cell.* 12:3668–3679.
- Zeng, G., and M. Cai. 1999. Regulation of the actin cytoskeleton organization in yeast by a novel serine/threonine kinase Prk1p. *J. Cell Biol.* 144:71–82.
- Zeng, G., X. Yu, and M. Cai. 2001. Regulation of yeast actin cytoskeleton-regulatory complex Pan1p/Sla1p/End3p by serine/threonine kinase Prk1p. *Mol. Biol. Cell.* 12:3759–3772.